Spatial distribution and formation mechanism of aeolian sand in the middle reaches of the Yarlung Zangbo River

LIU Yong[1,2]* https://orcid.org/0000-0003-2018-0144; ✉ e-mail: 1039786137@qq.com

WANG Yun-sheng[1] https://orcid.org/0000-0002-1774-9494; e-mail: wangys60@163.com

SHEN Tong[1] https://orcid.org/0000-0002-5075-5802; e-mail: 2276522564@qq.com

*Corresponding author

1 State Key Lab. of Geo-Hazard Prevention and Geo-Environment Protection, Chengdu University of Technology, Chengdu 610059, China

2 Institute of Exploration Technology, Chinese Academy of Geological Sciences, Chengdu 710043, China

Abstract: Aeolian sand landforms in the Yarlung Zangbo River (YZR) valley are a special type of aeolian landform that has attracted the attention of many scholars. However, the spatial distribution as well as the formation mechanism of aeolian sand has rarely been reported with integrated studies. In this paper, for remote sensing interpretation, scanning electron microscopy (SEM), X-ray diffraction (XRD) and particle size distribution (PSD) methods were used to analyze the spatial distribution and the deposition characteristics of aeolian sand. Combined with wind data and topography, the main driving factors and the formation mechanism of aeolian sand landforms were also examined. In the middle reaches of the YZR valley, there is a total of 2324.43 km² of aeolian sand, especially on the north bank of the wide valleys. In different wide valleys, the aeolian sand landforms exhibit a decreasing trend from the upstream to the downstream regions in both the area and expansion rate of aeolian sand. The cyclonic vortexes generated by the westerly winds and glacial winds are the main driving factors for transporting alluvial sand to the riverbank areas to form aeolian dunes. There are three main types of sand dunes in the river valley: climbing dunes, lee dunes and circumfluent dunes. Climbing dunes and lee dunes are mostly located west of the Jiacha Gorge, and the circumfluent dunes are mostly located east of the Jiacha Gorge.

Keywords: Aeolian processes; Remote sensing interpretation; Scanning electron microscopy; X-ray diffraction; Particle size distribution; Glacial winds; Cyclonic vortexes.

Introduction

In recent years, the origin and evolutionary process of aeolian landforms in the Yarlung Zangbo River (YZR) valley have become a research focus. Aeolian landforms in river valleys are mainly shaped by the environment of the valley, leading to a special type of aeolian geomorphology (Li et al. 1999; Draut 2012). Aeolian sand is mainly separated from the alluvial sand located on the sandbanks, floodplains and terraces (Li et al. 1997). Local wind systems shaped by valley topography are the driving force for aeolian processes (Bullard and McTainsh 2003). The aeolian sand source,

local wind and valley topographic are the most important factors controlling aeolian landforms (Bullard and Nash 1998). Influenced by aerodynamics and thermodynamics, a series of dynamic changes occur in the near-surface flow field, and the sand can be deposited in front or behind topographic obstacles. According to their location relative to the obstacles, aeolian landforms can be divided into two depositional modes: windward accumulations and leeward accumulations (Bagnold 1937; Zakrzews 1974; Mabbutt 1977). Haim Tsoar (1983) revealed that the shape of windward accumulations depends upon the slope and height of the obstacle based on wind tunnel simulations. The windward accumulations can be subdivided into echo dunes, which are single sand ridges formed parallel to vertical cliffs (Clos – Arceduc 1970), and featureless dunes, which climb gentle slopes (Evans 1962) and are known as climbing dunes. In the lee of the topographic obstacles, sand can be accumulated to form lee dunes (Smith 1968). The YZR valley is located in an alpine, high-altitude zone with a fragile ecological environment and long-term strong winds and drought conditions, which are conducive to the formation of aeolian sand landforms. Li et al. (1997) calculated the aeolian sand area to be 192 994.66 hm² in the YZR valley via aerial photographs, MSS Thematic Mapper (TM) satellite photographs and field investigations. Zhu (2012) found that aeolian sand is mainly accumulated in the middle reaches of the YZR. Zhou et al. (2014) found that the aeolian sand landforms are discontinuously distributed along the valley and identified three types of aeolian sand belts in the Milin valley of the YZR. Affected by sand sources and transport distance, the dune grain size becomes coarser and dune grain sorting becomes better in the downwind deposition area (Zhou et al. 2011). According to their geomorphological features, aeolian sand dunes can be divided into 21 categories, such as crescent dunes, transverse dunes, longitudinal dunes, pyramid dunes, etc. (Li et al. 1997). Li et al. (2010) found that the aeolian sand around Lhasa Airport located in the YZR Basin is mainly accumulated on the southern slope below 3800 m.

These and other studies have emphasized the morphometric characteristics and total amount of aeolian landforms. However, the spatial distribution and formation mechanism have been rarely studied, which is extremely disadvantageous to studying the evolution of the YZR valley. Here, one of the first systematic regional studies on the relevant geology, climate, geomorphology and land cover was conducted. Derived from detailed remote sensing interpretation, sample analysis and fieldwork, the spatial distribution and formation mechanism of the aeolian sand in the middle reaches of the YZR were analyzed.

1 Study Area

The YZR originates from the Majieyangzom glacier with an average elevation higher than 4000 m and is the highest river in the world. The river is located along the east-west fault zone between the Himalaya Mountains and the Gangdise Mountains and flows southward around Namjag Barwa Peak. According to the topographic characteristics of the river valley, the river basin can be divided into four wide valleys, namely, the Milin, Shannan, Shigatse and Maquan River wide valleys (Shen et al. 2012). The middle reaches of the YZR extend from Zhongba County in the west (30° 13′ N, 83° 14′ E) to the town of Pai in the east (29° 30′ N, 94° 52′ E) with a distance of approximately 1184 km (Figure 1). Aeolian sand landforms are mainly located in the wide valleys.

The YZR Basin is affected by both the plateau monsoon and the subtropical westerly jet, and the lower atmosphere exhibits two opposite temperature and pressure fields during a year. From May to September (summer), the southwest monsoon carries a large amount of water vapor through the lower reaches of the YZR. From October to April of the next year, the atmospheric circulation is dominated by cold high pressure, and westerly winds are frequent and strong in the basin (Li et al. 1999). The wind velocity can be extremely high, i.e., 40.8 m/s, and the number of windy days can reach 183 days per year.

The hydrologic data of the Yangcun hydrological station and Nuxia hydrological station from 1959 to 2014 reveal the seasonal variations in the flow and sand transportation of the YZR. The flood season is mainly concentrated from July to September, during which sand transport exceeds 90% of the annual average. In the dry seasons from

October to June of the next year, the water level of the YZR generally drops by 3 to 4 m (approximately 3 m in the wide valleys and ~6-8 m in the narrow valleys), and a large amount of alluvial sand is exposed from the water.

In the middle reaches of the YZR, the climate is extremely dry and cold, and there are only sparse populations of shrubs and herbs, such as Sophora pseudoacacia, artemisia and other grasses growing in the valley.

2 Materials and Methods

2.1 Remote sensing images and processing of aeolian sand landforms

A total of 136 remote sensing images from Gaofen-1 (GF-1) and Landsat in 1990, 2000, 2008, 2014, 2017 and 2018 were used in this study. The GF-1 remote sensing data taken in 2017 and 2018 are Panchromatic Multispectral Sensor (PMS) images with a spatial resolution of 8 m (except for band 1, which has a resolution of 2 m). The Landsat remote sensing data taken in 1990, 2000, 2008 and 2014 are TM images with a spatial resolution of 30 m (except for band 6, which is the thermal infrared band with a resolution of 120 m) (Table 1). All the remote sensing data for autumn and winter were used in the analysis. During these periods, precipitation is scarce, and clouds are rare. Therefore, the remote sensing images for these periods reflect the land covered by aeolian sand better than those of other periods.

ERDAS Imagine software version 9.2 was used to preprocess the remote sensing data. Using the least squares method and 1:100,000 topographic
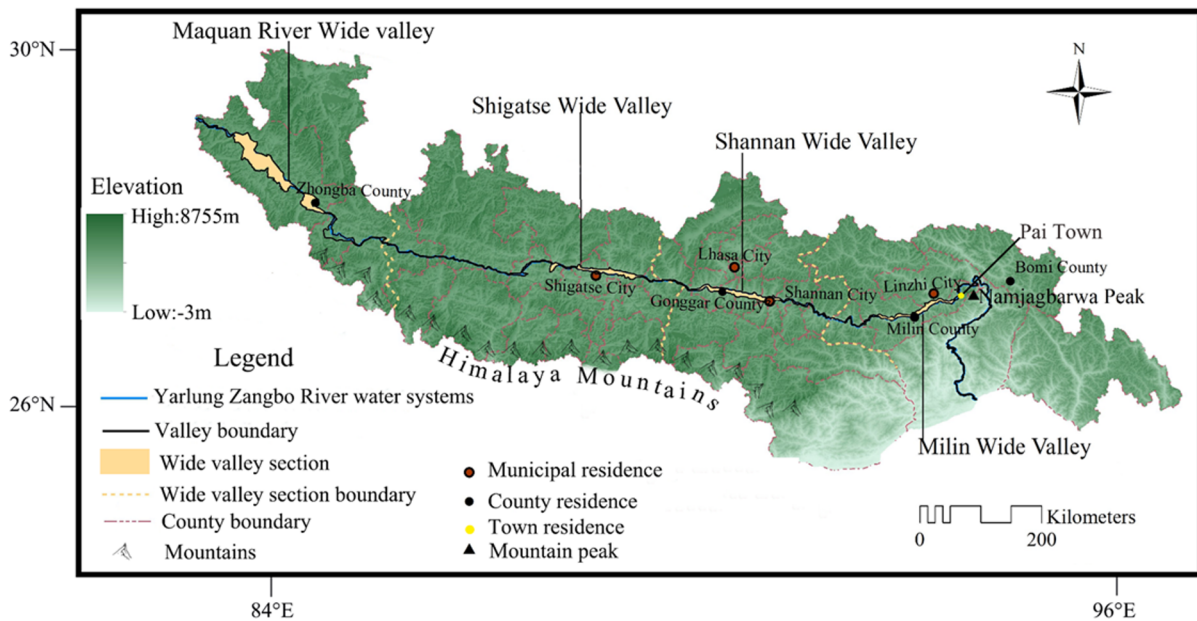

Figure 1 Location of the Yarlung Zangbo River basin in Tibet plateau.

Table 1 Relevant parameters of the remote sensing images

Remoting sensor	Band	Wavelength (µm)	Resolution (m)	Satellite	Acquisition time	Scenes
Panchromatic Multispectral Sensor (PMS)	1	0.45-0.90	2	Gaofen-1 (GF-1)	2017, 2018	72
	2	0.45-0.52	8			
	3	0.52-0.59				
	4	0.63-0.69				
	5	0.77-0.89				
Thematic Mapper (TM)	1	0.45-0.52	30	Landsat	1990, 2000, 2008, 2014	64
	2	0.52-0.60	30			
	3	0.63-0.69	30			
	4	0.76-0.90	30			
	5	1.55-1.75	30			
	6	10.40-12.50	120			
	7	2.08-2.35	30			

maps, all the remote sensing data were geometrically corrected. To ensure the accuracy of the geometric correction in each pixel, 20-30 ground control points were arranged for each scene. According to the dynamic analysis characteristics, the Albers coordinate system and Krasovsky ellipsoid were used. Because the sensors in the sky are often affected by the absorption, reflection and scattering of atmospheric components, such as molecules and aerosols, in the process of acquiring target terrain information, the remote sensing data include errors. Using the dark pixel method, the remote sensing data were atmospherically corrected. Combining RGB color synthesis and histogram matching, the corrected remote sensing data were used to construct the YZR Basin images with a consistent tone.

In the field surveys of the YZR Basin in 2016 and 2017, the location, distribution, surface tinges and textures of aeolian sand were recorded; the remote sensing images were compared with this information, and the fingerprints of aeolian sand in the remote sensing data were established. Unlike other landforms, aeolian sand is yellow-gray with fine texture and high albedo; thus, it can be easily distinguished from other landforms. Visual interactive interpretation was used to interpret the aeolian sand landforms manually from the remote sensing images with the help of ArcGIS 10.2 software.

To analyze the spatial variation trends in the observed aeolian sand landforms, typical aeolian sand ridge lines in the wide valleys of the Maquan River, Shigatse and Shannan were individually selected, and the positions of different periods were drawn on one map (no complete aeolian sand ridge line was found in the Milin wide valley) (Figure 2). Five points were evenly selected on each aeolian sand ridge line to calculate the average displacement and advancement rate of the ridges over the past 24 years.

2.2 Sample preparation and measurement techniques

Alluvial sand samples, aeolian sand samples and clayey sand samples collected in the Shannan wide valley were cleaned using 15% HCl (to remove carbonates) and 20% H_2O_2 (to remove organics). Then, the cleaned sand was used to generate measurement samples with an area of 5 mm × 5 mm. Using scanning electron microscopy (SEM), the morphological characteristics of the sand particles were observed. Field investigations conducted by Li et al. (1997) revealed that aeolian sand is mainly separated from alluvial sand. Thus, to clarify the source of aeolian sand in the study area, X-ray diffraction (XRD) was used to analyze the composition of both aeolian sand particles and alluvial sand particles. The scanning electron microscope used in this study was a HITACH X-650 with a maximum resolution of 5 nm; the acceleration voltage was selected at 15 kV. XRD was performed using a D/Max-3B made by the RigaKu Company of Japan; the continuous scanning speed as 0.3°/min, and the sampling interval was 0.02°. The X-ray spectra of the sand samples were compared with the powder diffraction file (PDF) provided by the Joint Committee on Powder Diffraction Standards – International Centre for Diffraction Data (JCPDS–ICDD) to analyze the sample composition.

Another 11 samples were collected at the 3 sample locations (As01-As03) near the Sangye Temple in the Shannan wide valley (Figure 3A). To clarify the aeolian sand particle size distribution
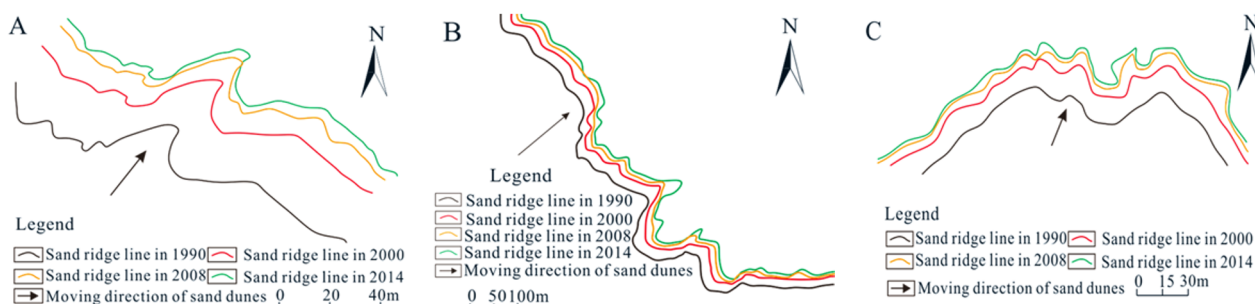

Figure 2 Moving trend of typical sand ridges. Sand ridge line A is located near Zhongba County of the Maquan River wide valley; sand ridge line B is located near Tubujia Country of the Shigatse wide valley; and sand ridge line C is located near Gonggar County of the Shannan wide valley. The three sand ridges are located on the northern bank of the Yarlung Zangbo River.

(PSD), the mean particle size (*Mz*) and separation coefficient (*δ*) were used as analysis indexes. *Mz* indicates the size of the sediment particles, which can reflect the transport capacity. The larger *Mz* is, the coarser the sediment particle size, reflecting a higher transport capacity. *δ* is mainly affected by weathering and pedogenic processes. The larger *δ* is, the worse the sorting, indicating that the sand has undergone stronger weathering and pedogenic processes (Zeng et al. 2007).

Folk and Ward (1957) deduced the following formulas of *Mz* and *δ* of sand particles:

$$Mz = \frac{\emptyset 16 + \emptyset 50 + \emptyset 84}{3} \quad (1)$$

$$\delta = \frac{\emptyset 84 - \emptyset 16}{4} + \frac{\emptyset 95 - \emptyset 5}{6.6} \quad (2)$$

where $\emptyset i$ is the particle size corresponding to *i*% on the cumulative probability curve of the sand sample. For convenience of comparison, the particle size units can be converted to *Φ*:

$$\Phi = \log_2 D \quad (3)$$

where *D* is the particle size in millimeters. GRADISTAT program (Blott and Pye 2001) was used to rapidly produce sediment grain-size statistics within excel. After inputting the percentage of sand present in a number of size fractions derived from a LS 13 320 XR laser diffraction granulometer, the sample statistical parameters such as *Mz*, *δ*, skewness and kurtosis were computed rapidly.

2.3 Data collection and analysis

Wind data were recorded from 1981 to 2010 at the Lazi meteorological station in the Maquan River wide valley, the Shigatse meteorological station in the Shigatse wide valley, the Gonggar meteorological station in the Shannan wide valley, and the Milin meteorological station in the Milin wide valley, as well as Nimu meteorological station at the periphery of the Shigatse wide valley and the Jiacha meteorological station at the periphery of the Shannan wide valley. The wind data were provided by the National Climatic Center of the China Meteorological Administration (NCCCMA). Each meteorological station records the meteorological factors every three hours. The average values from the Shigatse and Nimu meteorological stations were used as the meteorological factors in the Shigatse wide valley, and the average values for the Shannan and Jiacha meteorological stations were used as the meteorological factors in the Shannan wide valley.

Using field wind tunnel tests, Xie et al. (2018) measured the threshold wind speed of sand movement to be 5.0 m/s in the river basin of the Qinghai–Tibet Plateau. Referring to this threshold wind speed, average wind direction rose charts were used to calculate the wind for speeds exceeding 5 m/s in the dry season (Oct. to Apr. of the following year).

3 Results

3.1 Distribution of the current aeolian sand landforms

A total of 2324.43 km² of aeolian sand landforms are currently located in the study area. The aeolian sand landforms exhibit a banded and discontinuous pattern along the river valley, mainly distributed on the northern bank of the YZR, especially on the terraces, piedmont alluvial–diluvial plains, alluvial fans and mountain slopes of the wide valleys (Figure 4). In the Maquan River
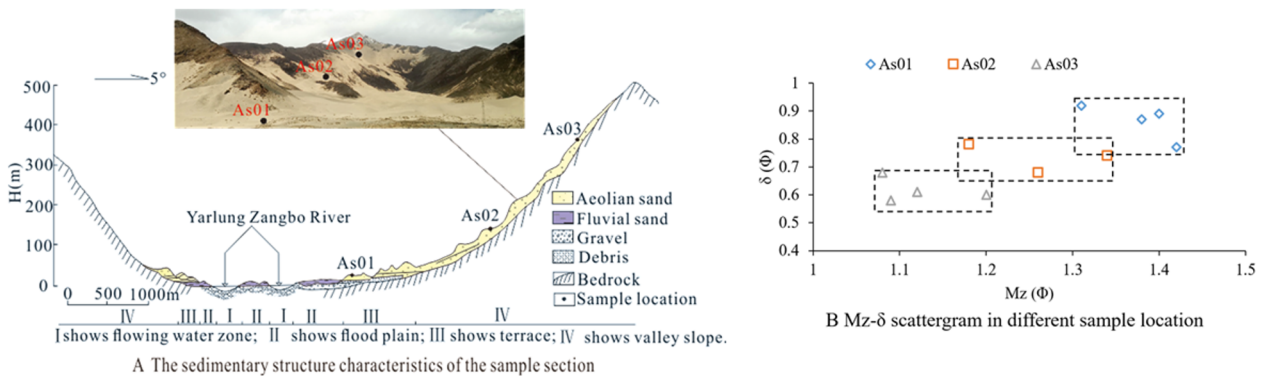

Figure 3 Characteristics of aeolian sand particles on the valley slope. *Mz*, mean particle size; *δ*, separation coefficient; *Φ*, particle size.
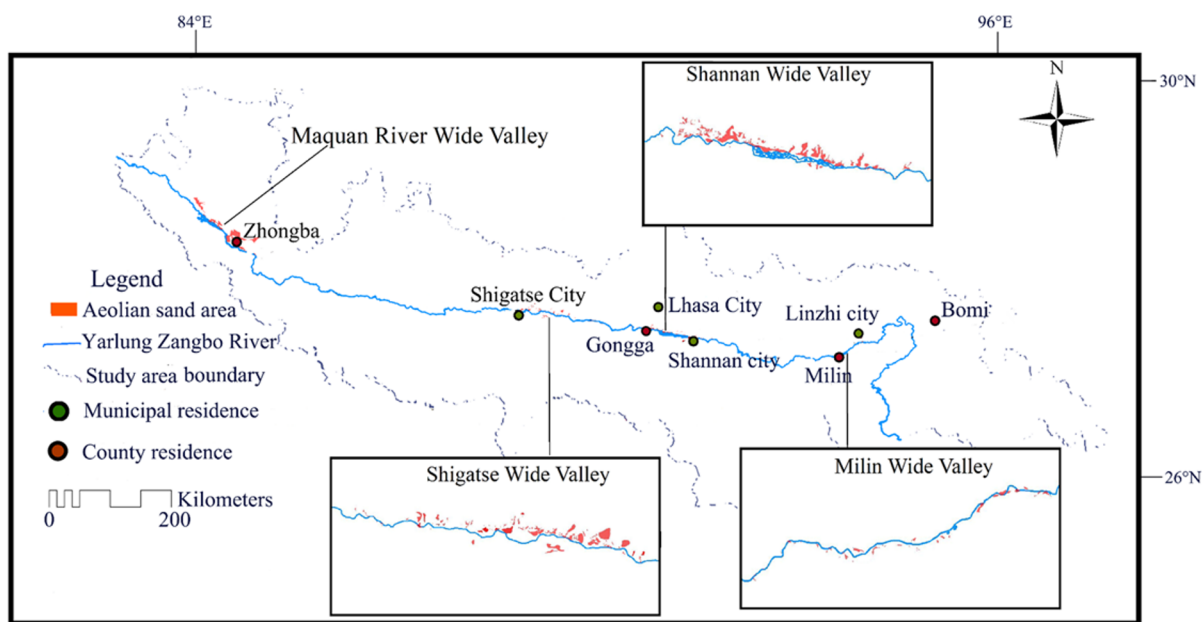
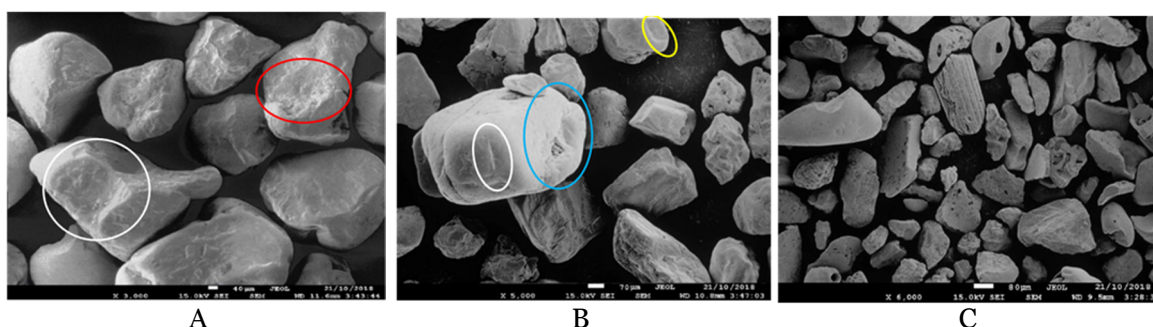**Figure 4** Aeolian sand land in the YarlungZangbo river valley.

Figure 5 Electron microscope photographs of typical sand materials. A shows fluvial sand; B shows aeolian sand; C shows clayed sand. Red circle shows conchoidal breakage; White circle shows V-shaped pit; Yellow circle shows round pit; Blue circle shows dish pit.

wide valley, Shigatse wide valley, Shannan wide valley and Milin wide valley, aeolian sand accounts for 1169.8 km², 593.82 km², 444.63 km² and 116.18 km², representing 50.33%, 25.55%, 19.13% and 4.99% of the total area, respectively, exhibiting a decreasing trend from upstream areas to downstream regions.

Three depositional modes of aeolian sand were identified: windward accumulations, leeward accumulations and circumfluent accumulations. The windward accumulations can be subdivided into echo dunes and climbing dunes. In the field investigations, echo dunes were not found in the study area, and climbing dunes are mostly distributed from the valley floor to an elevation of ~50-1500 m above the river. Generally, these climbing dunes exhibit flakes or strips on the slopes. The length of the climbing dunes is 35-1800

m, and the width is 15-1600 m. Barchans, transverse ridges and parabolic ridges are often found on the climbing dunes. In the lee of mountain slopes, sand accumulates to form lee dunes. Lee dunes are mostly connected to the climbing dunes and located on the leeward side of the ridges. Generally, the lee dunes are distributed in a small area of ~2000-600,000 m² and exhibit flakes on the slopes. Climbing and lee dunes are mainly located west of the Jiacha Gorge. When the near-surface wind surrounds a mountain spur, the carried sand can accumulate around the foot of the mountain to form a circumfluent dune. Most circumfluent dunes in the study area are located in the meandering valleys east of the Jiacha Gorge. Generally, the observed circumfluent dunes exhibit curved strips, with a width of ~5-120 m and length of ~500-2600 m.

3.2 Deposition characteristics of sand particles

The data shown in Figure 5, which were obtained via SEM, reveal that the sampled alluvial sand particles not only have different shapes but also have large differences in size. The alluvial sand particle diameters vary from 360 μm to 1400 μm. The alluvial sand particles are moderate to fine and subangular and subrounded in sphericity, with conchoidal breakage and V-shaped pits on the particle surfaces. The aeolian sand particles have a relatively higher sphericity, and many round pits, dish pits and V-shaped pits can be observed on the particle surfaces. The diameters of the aeolian sand particles range from 180 μm to 860 μm, and the sorting is relatively poor. The conchoidal breakage and V-shaped pits of the particles are mostly caused by water erosion. The round pits and dish pits show that the particles have undergone strong collisions, which most likely occurred in the process of wind transport. Thus, the aeolian sand particles have experienced not only wind transport but also river erosion. The sampled clayey sand particles are irregular subcircular in shape and have been strongly affected by chemical dissolution, with a large number of dissolution pits on the particle surfaces. The diameters of the clayey sand particles vary from 40 μm to 640 μm. Generally, the average size of the alluvial sand particles is the largest, followed by the aeolian sand particles, and the clayey sand particles have the smallest mean size.

The X-ray spectra of typical sand samples show that the composition and percentage of minerals in the aeolian sand particles are nearly the same as those in alluvial sand, indicating that the aeolian sand particles originated from alluvial sand (Figure 6). Compared with the PDF, quartz is the most abundant mineral in the two types of sand, accounting for more than half the total.

The statistical parameters of the aeolian sand samples taken near the Sangye Temple are shown in Figure 3B. Average particle size of As01 is 0.92-1.42 Φ, and the separation coefficient is 0.77-0.92 Φ. In As02, the average particle size is 1.18-1.34 Φ, the separation coefficient is 0.68-0.79 Φ. Average particle size of As03 is 1.08-1.21 Φ, and the separation coefficient is 0.58-0.67 Φ. Generally, particle size from As01 to As03 gradually decreases, and the separation coefficient also exhibits a decreasing trend. That is, with the increasing elevation, airflow transport capacity and weathering and pedogenic processes gradually decrease.

3.3 Spatial variation in the aeolian sand landforms

All of the selected aeolian sand ridges are located on the northern bank of the YZR, and the moving directions are from southwest to northeast (Figure 2). From 1990 to 2000, the advancement rate of the aeolian sand ridges was 2.03-2.47 m/a; from 2000 to 2008, the advancement rate was 0.97-1.54 m/a; and from 2008 to 2014, the advancement rate was 0.58-0.85 m/a. In general, after 2000, the advancement rate of the ridges decreased gradually. The average advancement rate of the aeolian sand ridges in the Maquan River, Shigaze and Shannan wide valleys were 1.75 m/a, 1.39 m/a and 1.32 m/a, respectively, decreasing
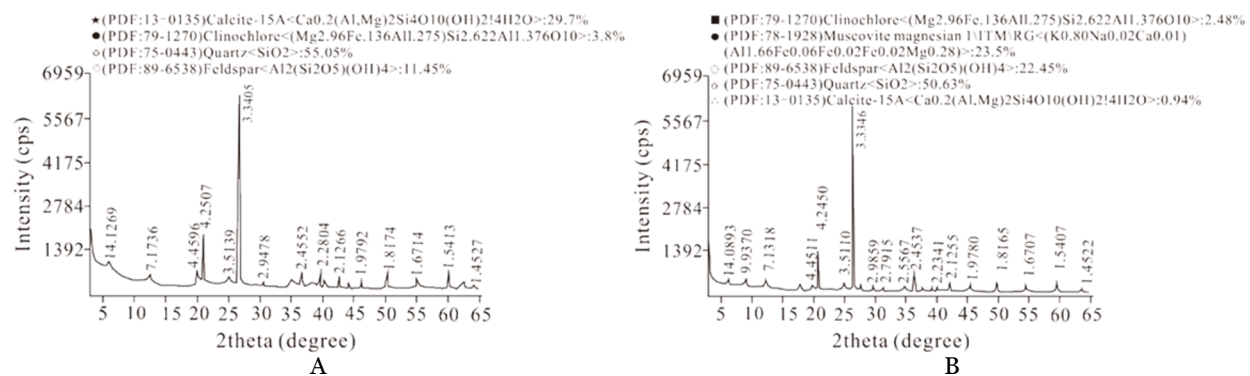

Figure 6 X-ray spectra of typical aeolian sand and fluvial sand. A shows aeolian sand; the quartz content is 55%, and the other mineral content is 45%. B shows fluvial sand; the quartz content is 50.6%, and the other mineral content is 49.4%.

from the Maquan River wide valley in the upstream area to the Shannan wide valley in the downstream area.

The area of aeolian sand in the four wide valleys has increased by different degrees in the past 24 years, as shown in Table 2. The rate of increase in the aeolian sand area in the various wide valleys is consistent with the moving trend of aeolian sand ridges. The increase from 1990 to 2000 was largest, followed by that of 2000-2008; the increase during the period 2008-2014 was the lowest. In the period 1990-2000, the annual increase rate of the aeolian sand area in the Maquan River valley was 7.99 km²/a, followed by that of the Shigaze wide valley (3.48 km²/a), the Shannan wide valley (1.48 km²/a), and the Milin wide valley (1.32 km²/a). The order of increase in the four wide valleys in 2000-2008 and 2008-2014 were the same as that in 1990-2000.

3.4 Wind regime of the study area

The annual average wind velocity in the Maquan River, Shigatse and Shannan wide valleys exhibited a decreasing trend from 1981 to 2010. The long-term average wind velocity decreases from the Maquan River wide valley in the upstream area to the Milin wide valley in the downstream area (Figure 7). Wind speeds exceeding 5 m/s at the Lazi, Shigatse, Nimu, and Gonggar meteorological stations are controlled by southwesterly winds, and the frequencies of wind directions between 180° and 270° are 48%, 56%, 45% and 50%; wind speeds exceeding 5 m/s at the Jacha and Milin stations are controlled by southeasterly winds, and the frequencies of wind directions between 90° and 180° are 46% and 41% (Figure 8). Generally, southerly winds prevail in the middle reaches of the Yarlung Zangbo River Basin during the dry seasons. From the hourly meteorological data recorded by the meteorological stations, the wind velocity in the four wide valleys is relatively low from dawn to approximately 15:00 p.m., and then the velocity increases gradually until late at night. Strong winds often occur in the period from afternoon to late night.

4 Discussion

Table 2 Aeolian sandy land area of the four wide valley sections

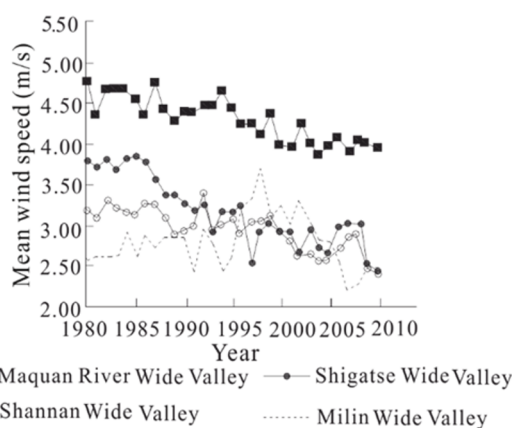| Time	Aeolian sandy land area of wide valley (km²)			
	Maquan River	Shigatse	Shannan	Milin
1990	1066.34	539.36	419.54	95.91
2000	1146.24	574.14	434.25	109.14
2008	1160.08	585.94	440.49	113.3
2014	1169.8	593.82	444.63	116.18

Figure 7 Variations in annual mean wind speed of the four wide valleys.

4.1 Evolution process of the driving wind

Blocked by the Himalayas, the Indian Ocean Current only moves from downstream to upstream along the YZR valley, resulting in abundant rainfall and warm climate in the lower reaches of the YZR. The wind regime in the Milin wide valley is also affected by the Indian Ocean Current coming from the east. In the upper and middle reaches of the river, the plateau monsoon and the subtropical westerly jet play important roles in winter and spring, leading to westerly winds prevailing in the river basin.

When the airflow traverses the river valley, the central wind speed of the valley is the highest. Under the action of friction, the wind speed decreases gradually from the center to the slopes on both sides, forming notable horizontal wind shear. This shear can be expressed by the relative vorticity formula in a natural coordinate system:

$$\zeta = \frac{V}{R_S} - \frac{\partial V}{\partial n} \qquad (4)$$

where the relative vorticity (ζ) is composed of the curvature vorticity ($\frac{V}{R_S}$) and shearing vorticity ($-\frac{\partial V}{\partial n}$), V is the wind speed, and R_S is the radius of curvature. In a straight river valley, the radius of
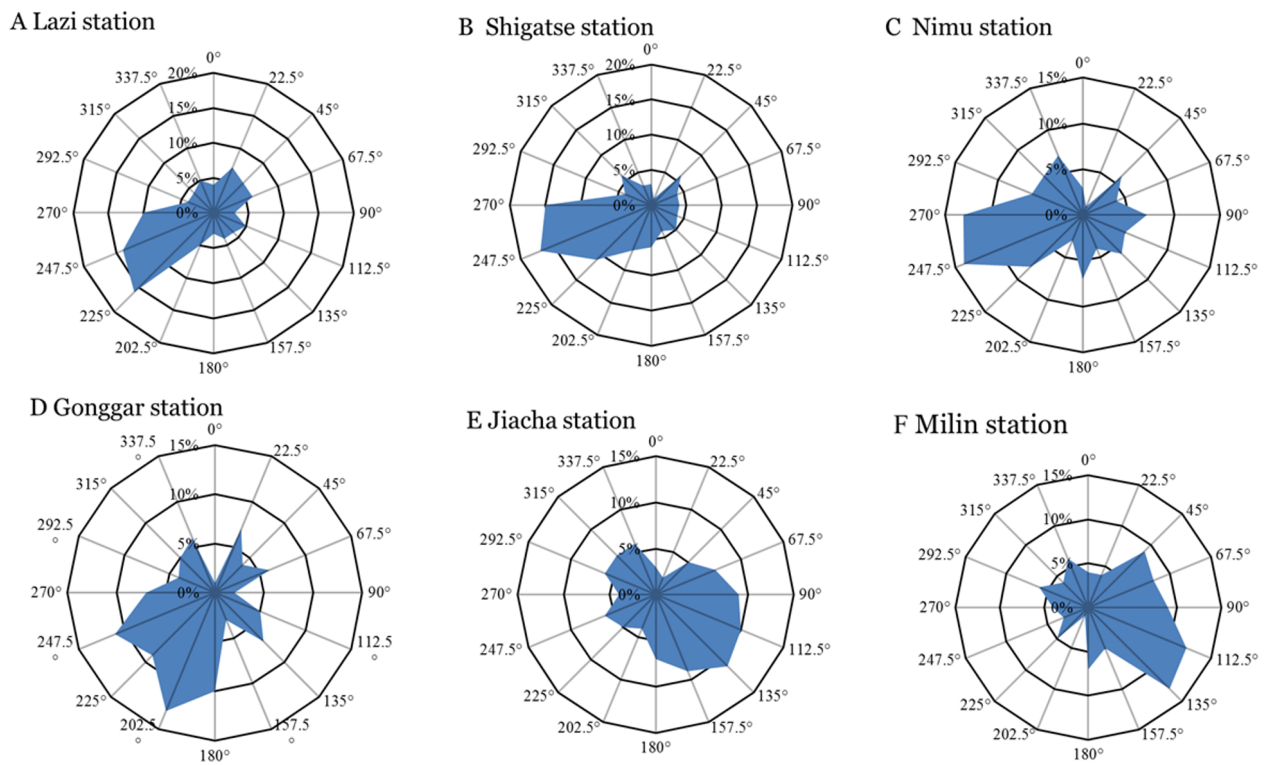
Figure 8 Rose charts of the average wind direction, averaged over October to April of the following year.
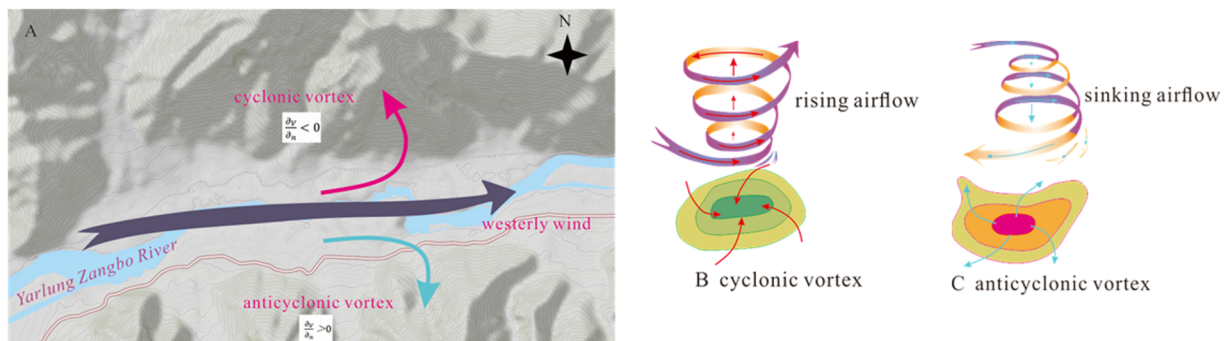

Figure 9 Diagram of the formation of cyclones and anticyclones on both sides of the valley. Cyclones occur primarily on the northern bank of the valley, and anticyclones occur primarily on the southern bank.

curvature (R_S) is infinite, so the curvature vorticity ($\frac{V}{R_S}$) can be neglected; the relative vorticity can also be expressed as follows:

$$\zeta = -\frac{\partial V}{\partial n} \qquad (5)$$

The study area is located in the Northern Hemisphere. When westerly winds traverse the river valley, the relative vorticity on the northern bank exceeds 0, i.e., $\frac{\partial V}{\partial n} < 0$ and $\zeta > 0$, which is conducive to the formation and development of cyclonic vortexes that can promote rising motion; the relative vorticity on the southern bank is less than 0, forming anticyclonic vortexes that promote sinking air (Figure 9). Under the action of rising air, alluvial sand is more easily transported to the riverbank to form aeolian sand.

The Himalayas are situated on the south side of the YZR, and a large number of perennial glaciers cover the northern slopes (with an average altitude of 2600 m above the YZR). Due to the high albedos of the glaciers, a large amount of solar radiation can be reflected into space, causing the air above the glaciers to absorb less energy. Thus, the airflow on the northern slopes of the Himalayas

is colder and denser than elsewhere. Due to the continuously sloping topography and "Ekman pumping", the airflow on the northern slopes of the Himalayas flows downhill along the glaciers to form strong glacial winds (Figure 10A).

In the YZR valley, due to the large specific heat capacity of water, a large amount of solar radiation is absorbed by the river, resulting in the air originating over the river having a lower temperature than that on the valley slopes. Therefore, the cold air over the river surface sinks to form a high-pressure area, and the warm air over the valley slopes rises to form a low-pressure area, ultimately creating an anabatic wind blowing from the river to the valley slopes (Figure 10B).

At night, due to the lack of solar radiation, air originating from the river surface is much warmer than that over the valley slopes. Thus, the air pressure above the river surface is lower than that over the valley slopes, forming a katabatic wind blowing from the valley slopes to the river (Figure 10C). The katabatic wind can enhance the glacial winds at night.

Due to the large number of glaciers on the northern slopes of the Himalayas and the large decrease in altitude of the glacial winds blowing to the river, the glacial winds are very strong and play an important role in the mountain-valley winds of this region. As a result, southerly winds prevail in the YZR valley (especially in the wide valleys from afternoon to late at night), and the average wind speed decreases from the Maquan River wide valley in the upstream area to the Milin wide valley in the downstream area.

Under the action of cyclonic vortexes and southerly winds, alluvial sand was primarily transported to the northern bank of the wide valleys to form aeolian sand, and the aeolian sand region in the wide valleys exhibits a decreasing trend from the upstream area to the downstream region.

4.2 Formation mechanism of the aeolian sand landforms

Affected by topography and wind, aeolian sand was mainly deposited in three ways: windward accumulations, leeward accumulations and circumfluent accumulations.

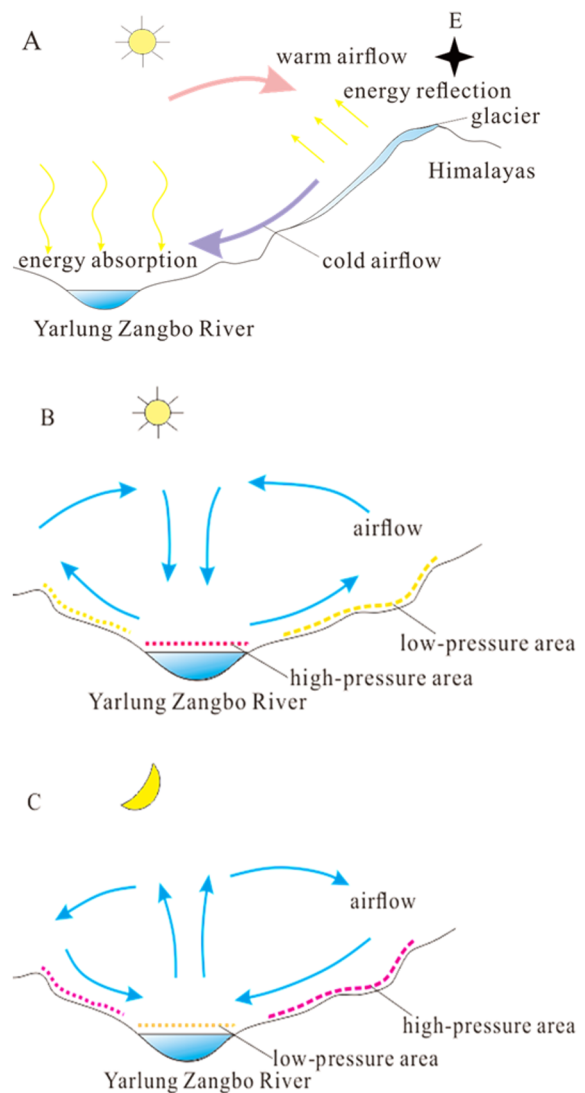### 4.2.1 Windward accumulations

Figure 10 Schematic diagram of wind formation. A shows glacial wind; B shows mountain-valley wind during the day; C shows mountain-valley wind at night.

Windward accumulations depend on the slope of the obstacle. These deposits can be subdivided into climbing dunes and echo dunes. According to Haim Tsoar's (1983) wind tunnel modeling study, when airflow approaches slopes of 50° and lower perpendicularly, the air simply rises and flows over the gentle slopes, the wind speed at the foot of the slope is lowest, and the sand transported by the airflow accumulates on the foot of the slope. Under the action of airflow, a large amount of sand accumulates gradually from the slope foot to the slope surface to form climbing dunes (Figure 11A-C). When the airflow approaches a cliff perpendicularly (slope generally exceeding 50°),
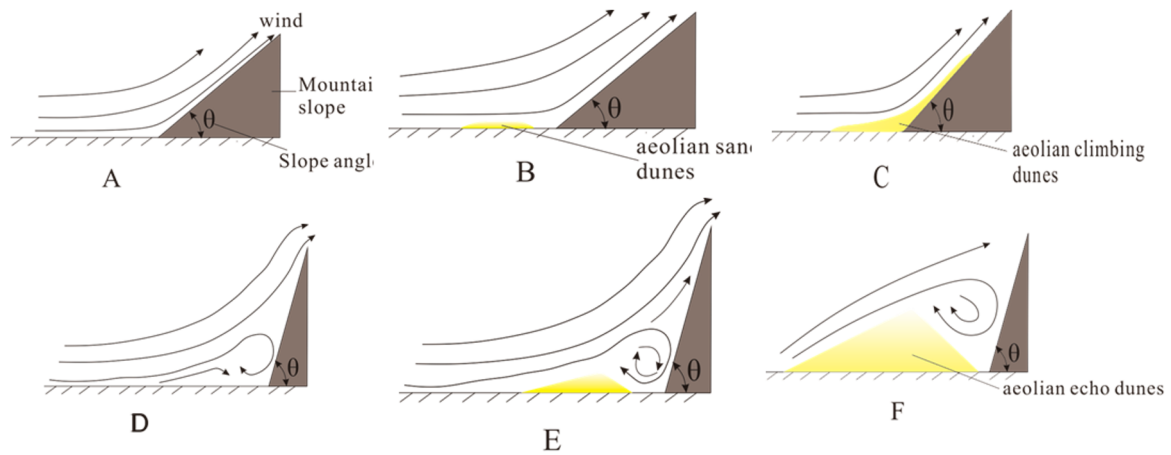
Figure 11 Tracks of airflow in front of and over different slopes: A-C - gentle slope; D-F - steep slope.
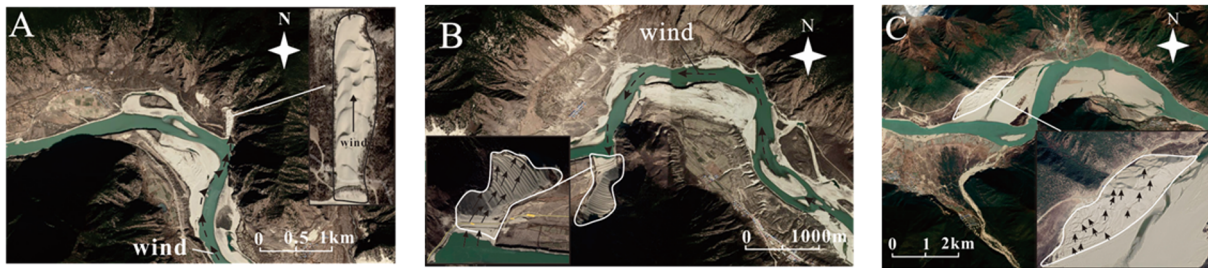

Figure 12 Typical climbing dunes. A shows the climbing dune on a gentle slope; B shows the climbing dune on a steep slope; C shows the climbing dune affected by different winds.

the air slows down with a consequent increase in pressure against the face (Eaton 1980). As a result, the airflow begins to separate from the floor. Some of the air rises and flows over the cliff, while the remaining air makes a loop and creates a reverse-flow eddy in front of the cliff. Thus, air moving in opposite directions occurs at the front of the cliff, which results in a lowering of the wind velocity and deposition. A large amount of sand can be deposited to form echo dunes in front of the cliff under these conditions (Figure 11D-F). In the field investigation performed in this study, the climbing dunes are the main windward sand dune type in the study area. A special climbing dune covered by crescentic ridges and compound crescentic ridges is located on a concave slope on the northern bank of the river valley (29° 10.1′ N, 93° 37.8′ E) (Figure 12A). In the SSE-NNW direction, the sand dune climbs up the mountain slope from the floodplain, with a maximum elevation of 394 m above the river. The sand dune has a mean length of 705 m, a mean width of 127 m, an area of 89535 m², and a mean slope of 34°. Our measurements indicate that the driving winds of the climbing sand dune are mainly affected by the topography of the valley. When the

wind blows along the valley from the east, affected by the bending terrain of the valley, the wind turns to the northwest. Blocked by the depression of the northern bank valley slope, the wind slows down, and the sand transported by the valley wind is deposited on the mountain slope.

When the wind blows diagonally toward a steep mountain slope, the air rises and flows around the slope. Blocked by the slope, the wind slows down, and the sand transported by the wind is deposited on the steep slope to form a climbing dune. For example, one specific climbing dune is located on the western slope of a mountain spur (the slope is 62°) inside a meandering channel on the right-hand side of the river valley (29° 8.4′ N, 94° 40.2′ E) (Figure 12B). The sand dune originates from the floodplain and climbs up the concave mountain slope following a NNE–SSW direction, with a maximum elevation of 504 m above the river, a length of 734 m, and a width of 216 m. There are many vertical sand ridges superimposed on the surface of the climbing dune parallelly, indicating that the sand dune has experienced northeasterly winds rising and flowing around the slope. When the wind blows from east

to west, the wind turns to the southwest due to the meandering river valley topography, and the alluvial sand is transported from the floodplain to the mountain slope to form a climbing dune.

Climbing dunes can also be affected by different winds in different directions during their formation process, such as the famous Danniang dune (29°2.8′ N, 94°4.1′ E) (Figure 12C). This sand dune is located at the foot of the mountain slope with a mean length of 2.2 km and a mean width of 614 m. It is high in the middle and low at both sides, similar in appearance to Buddha's palm. The shapes of the barchans and transverse ridges on the surface of the sand dune indicate that the sand dune has experienced the action of southwesterly and southeasterly winds. This phenomenon should be related to the different prevailing winds in the different seasons in the river valley. Influenced by both topographic and atmospheric circulations, the dominant wind differs in different river sections and periods. Therefore, many dunes are not affected by a single wind, and sand ridges with different shapes can be formed on the sand dune surface.

4.2.2 Leeward accumulations

When air flows over an obstacle, the sand transported by the air accumulates in the lee of the obstacle to form lee dunes. According to the wind tunnel simulations by Greeley et al. (1974), the airflow is accelerated on the windward slope and reaches its maximum speed at the top of the obstacle. The airflow speed at the top can be 1.1-2.0 times higher than that at the bottom of the slope. After flowing over the top of the obstacle, the airflow separates on the lee side. Some air

continues to move in the original direction, while the remaining air generates separation vortexes and secondary flows (Frank 1996; Walker 2003) (Figure 13A). Blocked by the lee side of the slope, the secondary flows slow down, and the sand transported by the secondary flows is deposited on the lee side of slope to from a lee dune (Figure 13B). In the study area, one specific lee dune (29°21.6′ N, 90° 55.8′ E) is located on the northern bank of the YZR, with a length of 846 m and a width of 750 m (Figure 13C). Covered on the top of a mountain slope, the lee dune is connected to a climbing dune. The climbing dune originates from the foot of the mountain to the top, and the sand ridges on the surface indicate that the climbing dune has experienced a northwesterly wind. The sand ridges on the lee dune indicate that the lee dune has experienced a southeasterly wind that is opposite to the climbing dune. Thus, a northwesterly wind prevails in this area, and the southeasterly wind affecting the lee dune must originate from secondary flows of the driving wind of the climbing dune. The shape of the lee dune is controlled by the secondary flows generated by the air passing over the obstacle.

4.2.3 Circumfluent accumulations

After the near-surface airflow bypasses the mountain spur, the air separates on the concave bank of the mountain. Some air continues to move in the original direction, while the remaining air generates secondary flows to form cyclonic circulation (Haim Tsoar 1983). Under the action of mountain friction, this cyclonic circulation slows down, and the sand transported by the circulation is deposited on the foot of the mountain to form
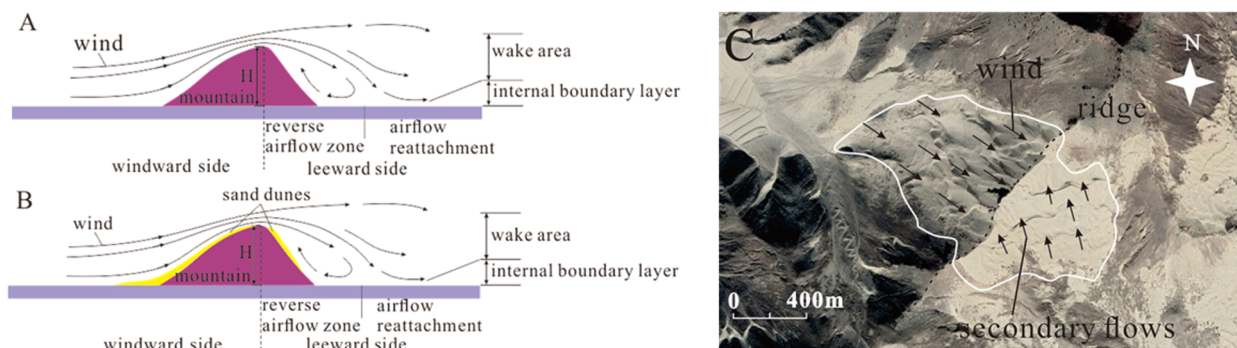

Figure 13 Typical lee dunes. A shows the characteristics of flow over an obstacle; B shows the sedimentary characteristics of dunes on both sides; C shows the details of the surface shape of a lee dune.
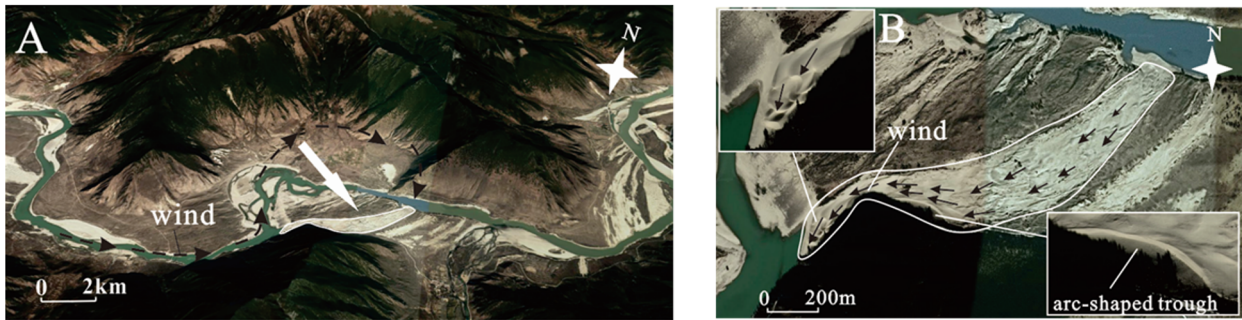
Figure 14 Typical circumfluent dunes. A shows the location of the circumfluent dune; B shows details of the surface shape and driving wind of the dune.

circumfluent dunes. A typical circumfluent dune is located near Linong township, Linzhi city (29°7.8′ N, 93°51′ E) inside a meandering channel on the right-hand side of the riverbank (Figure 14A). The river section where the circumfluent dune is located is approximately semicircular. When the wind blows from west to east along the river section, the wind is blocked by the topography of the northern depression and develops into a northeasterly wind in the lower reaches of the river section, resulting in a large amount of sand being deposited on the terrace slope and the foot of the mountain. There is an arc-shaped trough with an average length of 351 m, an average width of 75 m and an average height of 2.3 m located at the front edge of the mountain (Figure 14B). The arc-shaped trough may be caused by wind erosion. According to the wind tunnel tests carried out by Cheng et al. (2003), when blocked by obstacles, air will decelerate at the front of obstacles and flow to one side. As a result, with the gradual accumulation of air around the side, the wind speed along the edge of the mountain increases rapidly. Under the combined action of high wind speeds along the edge of the mountain and northeasterly winds, an arc-shaped high wind speed belt is formed at the edge of the mountain, which is not conducive to the deposition of sand particles. After the air bypasses the mountain spur, a cyclonic circulation is formed on the concave bank of the mountain, causing the sand transported by the airflow to deposit on the foot of the concave slope and forming a circumfluent dune.

In the middle reaches of the YZR, west of the Jacha Gorge, the river valley is relatively straight, and the mountain slopes of the wide valleys are relatively gentle, resulting in many climbing dunes

and lee dunes on the mountain slopes; east of the Jacha Gorge, the valley is meandering and winding, resulting in many circumfluent dunes located at the foot of the mountain slopes.

5 Conclusion

In this study, remote sensing interpretation, SEM, XRD and PSD methods were identified for estimating the spatial distribution and deposition characteristics of aeolian sand, and the main driving factors and the formation mechanism of aeolian sand landforms were obtained and discussed. The conclusions are as follows.

(1) The glacier wind from the Himalayas and the subtropical westerly jet are the primary driving factors for the presence of aeolian sand, which mostly transport the alluvial sand to the northern bank of the wide valleys to form aeolian sand. The aeolian sand landforms exhibit decreasing trends from the upstream region to the downstream region with regard to area and expansion rate. From 1990 to 2000, the expansion rate of aeolian sand increased gradually. After 2000, the expansion rate began to decline.

(2) Due to the gradual decrease of the airflow transport capacity with elevation, the aeolian sand particle size decreases gradually from the alluvial flats to higher locations on the valley slopes.

(3) Aeolian sand deposition in the middle reaches of the YZR valley could well be described by windward accumulations, leeward accumulations and circumfluent accumulations. All the sand accumulations are shaped by obstacle and local wind. So, circumfluent accumulations are mostly located in the meandering and winding valley

east of the Jiacha Gorge, windward accumulations and leeward accumulations are distributed in the straight valley west of the Jiacha Gorge.

As the climate warms, the glaciers on the Himalayas will gradually melt, and the glacial winds will gradually weaken, resulting in a decrease in the rate of aeolian sand expansion and the aeolian sand particle size in the YZR valley.

References

Bullard JE, Mc Tainsh GH (2003) Aeolian–fluvial interactions in dryland environments: examples, concepts and Australia case study. Progress in physical geography 27(4): 471-501. https://doi.org/10.1191/0309133303pp386ra

Bullard JE, Nash DJ (1998) Linear dune pattern variability in the vicinity of dry valleys in the southwest Kalahari. Geomorphology 23(1): 35-54. https://doi.org/10.1016/S0169-555X(97)00090-1

Blott SJ, Pye K (2001) GRADISTAT: a grain size distribution and statistics package for the analysis of unconsolidated sediments. Earth Surface Processes and Landforms 26(11): 1237-1248. https://doi.org/10.1002/esp.261

Bagnold RA (1937) Recent explorations in the desert (1932 – 1936). Geographical Journal 89(3): 265-268.

Clos - Arceduc A (1970) The use of aerial photographs in the study of the lengthening of sand dunes in a direction close to that of the wind, in the Sahara. Photogrammetria 25(5-6): 189-199. https://doi.org/10.1016/0031-8663(70)90006-2

Cheng X (2003) Experimental Research on Sand Incipience Law in Wind-blown-sand Two Phase Flow. PhD thesis, Tsinghua University, Beijing, China. p 48. (In Chinese)

Draut AE (2012) Effects of river regulation on aeolian landscapes, Colorado River, southwestern USA. Journal of GeophysicalRresearch 117(2): 1-22. https://doi.org/10.1029/2011JF002329

Evans JR (1962) Falling and climbing sand dunes in the Cronese ("Cat") Mountain Area, San Bernadino County, California. The Journal of Geology 70(1): 107-113. https://doi.org/10.1086/626798

Eaton KJ (1980) Low – income housing and hurricanes. Wind Engineering 1: 7-21.

Folk RL, Ward WC (1957) Brazos reviver bar - a study in the significance of grain size parameters. Journal of Sedimentary Petrology 27(1): 3-26.

Frank A, Kocurek G (1996) Towards a model for airflow on the lee side of aeolian dunes. Sedimentology 43: 451-458. https://doi.org/10.1046/j.1365-3091.1996.d01-20.x

Greeley R, Iversen JD, Pollack JB, et al. (1974) Wind tunnel simulation of light and dark streaks on Mars. Science 183(4127): 847-849. http://doi.org/10.1126/science.183.4127.847

Tsoar H (1983) Wind tunnel modeling of echo and climbing dunes. Developments in Sedimentology 38: 247-259. https://doi.org/10.1016/S0070-4571(08)70798-2

Li S, Dong GR, Shen JY, et al. (1999) Formation mechanism and development model of aeolian sandy landform in Yarlung Zangbo River Valley. Science in China (Series D) 29(1): 88-96. (In Chinese)

Li S, Wang Y, Ha S, et al. (1997) Classification and development of aeolian sand landform in the Yarlung Zangbo Valley. Journal of Desert Research 17(4): 342-350. (In Chinese)

Li HD, Shen WS, Zou CX, et al. (2010) Spatial distribution and evolution of aeolian sandy land in the areas around Lhasa Airport (Tibet，China) since 1990. Acta Ecologica Sinica 30(21): 5716-5727. (In Chinese)

Mabbutt JA (1977) Desert Landforms, Canberra, Australian. Australian National University Press. p 340.

Smith HTU (1968) Chapter III – Geologic and Geomorphic Aspects of Deserts. In: Desert Biology. pp 51-100.

Shen WS, Li HD, Sun M, et al. (2012) Dynamics of aeolian sandy land in the Yarlung Zangbo River basin of Tibet, China from 1975 to 2008. Global and Planetary Change 86-87: 37-44. https://doi.org/10.1016/j.gloplacha.2012.01.012

Walker I, Nickling WG (2003) Simulation and measurement of surface shear stress over isolated and closely spaced transverse dune in a wind tunnel. Earth Surface Processes and Landforms 28(10): 1111-1124. https://doi.org/10.1002/esp.520

Xie SB, Yu WB, Qu JJ, et al. (2018) Dynamic Environment of Blown Sand at Honglianghe River of Qinghai-Tibet Plateau. Journal of Desert Research 38(2): 219-224. (In Chinese)

Zhu S (2012) River Landform and Geology Environment Evolution in the Yarlung Zangbo River Valley. PhD thesis, Chinese Academy of Geological Sciences, Beijing, China. p 77. (In Chinese)

Zhou N, Zhang CL, Wu XX, et al. (2014) The geomorphology and evolution of aeolian landforms within a river valley in a semi-humid environment: A case study from Mainling Valley, Qinghai–Tibet Plateau. Geomorphology 224: 27-38. https://doi.org/10.1016/j.geomorph.2014.07.012

Zhou N, Zhang CL, Liu YG (2011) Variation of Grain Size on Surface of Barchans in Maiming Great Valley, Yarlung Zangbo River. Scientia Geographica Sinica 31(8): 958-963. (In Chinese)

Zeng LH, Li S, Li BS, et al. (2007) The Genesis and Environmental Significance of the Sandy Sediments of the Upper Basuo Formation in Western Hainan Island. Geological Review 53(6): 783-791. (In Chinese)

Zakrzews B (1974) Geomorphology in Deserts – Cooke RU and Warren A. Professional Geographer 26(4): 455-456.